INTERPORE 2026

Structure-Driven Design of Porous Electrodes for improving Fast Charging and Energy Capacity (or capacitance) *for Batteries and Supercaps*

A Structure-Transport-Driven Framework for Optimizing Laser-Engineered 3D Porous Electrodes

Structure-resolved transport analysis and optimization of laser-engineered porous electrodes

Nadia Bali

Michael Athanasiou

Spyros N. Yannopoulos*

Fast charging is a transport problem

- High charging rates require rapid ion transport
- Complex pore pathways create bottlenecks
- Poor accessibility reduces usable capacity

Battery

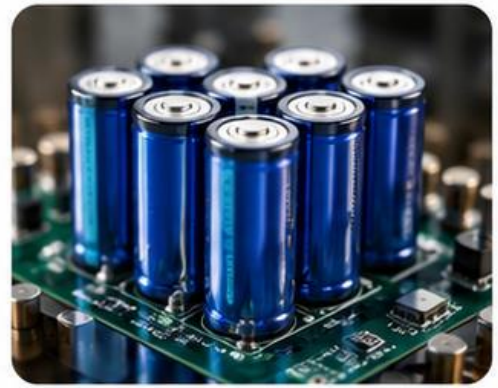

EDLC Supercapacitors

Plan Action: Batteries (cell – level)		Current	Target 2030 US	Target 2030 EU
Voltage	Advanced LIB cells (e-mobility)	4.0–4.5	4.5–5.0 V	4.5 – 5.0 V
Gravimetric energy density		90–235 Wh kg^{-1}	≥ 400 Wh/kg	≥ 400 Wh kg^{-1}
Gravimetric power density		250–340 W kg^{-1}	≥ 400 Wh/kg	> 700 W kg^{-1}
Cycle life		5000–6000	≥ 1,000–1,500 cycles at 80% DoD	> 15000 cycles
Cost		150–120 € kWh^{-1}	≤ $60/kWh	< 100 € kWh^{-1}
Gravimetric energy density		35 Wh kg^{-1}		45 Wh kg^{-1}
Recyclability			> 90% material recovery rate	> 90% material recovery rate
Fast Charging		80% charge in = 40′	80% charge in < 15′	80% charge in < 20′
Improvement by Laser Engineer Restructuring		80% charge in 30 minutes		

Image with an electric car

Key References

Weiss, M. et al. Fast Charging of Lithium-Ion Batteries: A Review of Materials Aspects. Adv. Energy Mater. 11, 2101126 (2021).

Tomaszewska, A. et al. Lithium-Ion battery fast charging: A review. eTransportation 1, 100011 (2019).

Liu, Y., Zhu, Y. & Cui, Y. Challenges and opportunities towards fast-charging battery materials. Nat. Energy 4, 540–550 (2019).

Porosity alone cannot describe transport

Classical effective-medium models assume:

- Homogeneous pores
- Isotropic transport
- Smooth connectivity

EFFECTIVE-MEDIUM EQUATION

$$D_{eff} = D_0 \cdot \varepsilon^a$$

WHY THE MODEL BREAKS

Slit-like pores
geometry violates the spherical-pore assumption

Structural disorder
heterogeneous connectivity, not captured by a single exponent

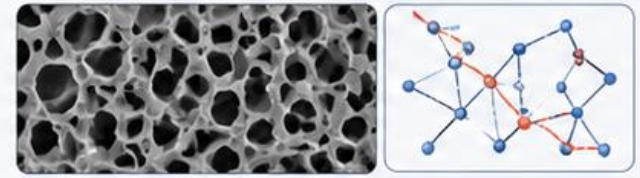

Effective Diffusivity: Two-Phase Composite vs Simple Bruggeman (1st-order)

Comparison for known D_1, D_2, ϕ_1, ϕ_2

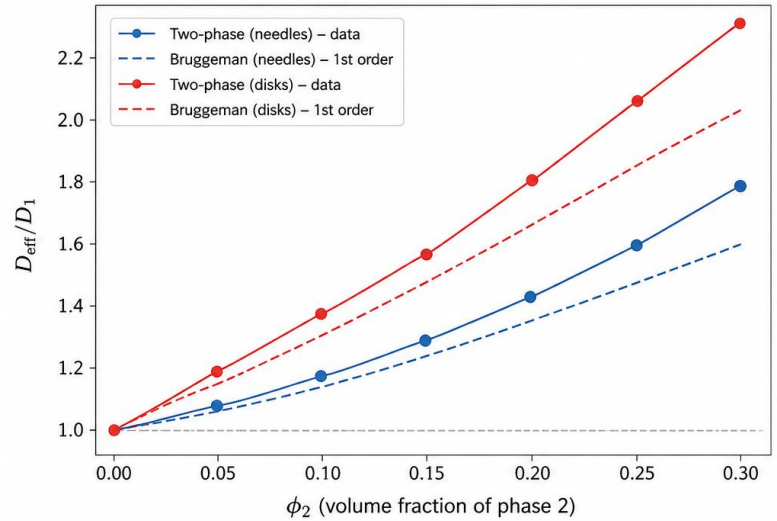

Simple Bruggeman (1st order in ϕ_2)

Needles (spheroids, $a \gg b$)

$$\frac{D_{\text{eff}}}{D_1} = 1 + \frac{(D_2 - 5D_1)(D_2 - D_1)}{3D_1(D_2 + D_1)}\,\phi_2 + \mathcal{O}(\phi_2^2)$$

Disks (oblate spheroids, $a \ll b$)

$$\frac{D_{\text{eff}}}{D_1} = 1 + \frac{(2D_2 + D_1)(D_2 - D_1)}{3D_1 D_2}\,\phi_2 + \mathcal{O}(\phi_2^2)$$

Observation

- Disks configuration yields higher D_{eff} than needles for $D_2 > D_1$.
- Bruggeman 1st-order expressions capture the initial trend, with increasing deviation at higher ϕ_2.
- The disparity grows with ϕ_2 due to higher-order terms in the effective medium expansion.

Parameter values (example)

$D_1 = 1.0 \times 10^{-10}$ m^2/s	$D_2 = 1.0 \times 10^{-9}$ m^2/s	$\phi_1 = 1 - \phi_2$	$\phi_2 \in [0,\ 0.30]$
(matrix)	(inclusion)	(volume fraction)	(volume fraction of phase 2)

Note: Two-phase data obtained from 3D microstructure-based transport simulations (48 images).

Key References

Eberle, M., Chung, D.-W., García, R. E. & Wood, V. Tortuosity Anisotropy in Lithium-Ion Battery Electrodes. *Adv. Energy Mater.* 4, 1301278 (2014).

Tjaden, B. et al. On the origin and application of the Bruggeman correlation for analysing transport phenomena in electrochemical systems. *Curr. Opin. Chem. Eng.* 12, 44–51 (2016).

Thorat, I. B. et al. Quantifying tortuosity in porous Li-ion battery materials. *J. Power Sources* 188, 592–600 (2009).

Research questions

1. Does pore architecture directly control fast charging?

2. Which structural descriptors govern transport?

3. Can porous electrodes be computationally optimised?

VISUAL CUE

Supercapacitors: *Tortuosity and directional transport shows how geometry steers ion pathways across in-plane and through-plane directions.*

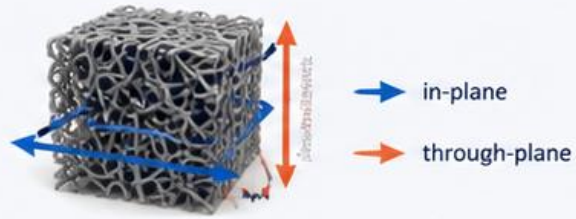

Batteries: *Li intercalation process highly depend on porous media.*

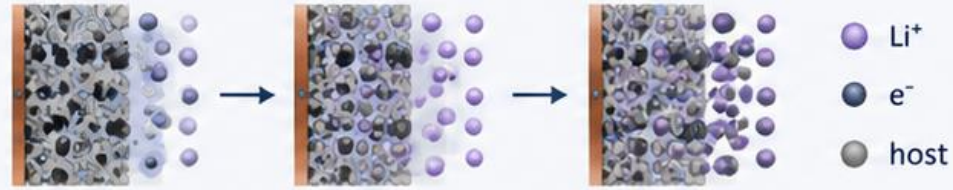

(i) Electrolyte infiltration

(ii) Li^+ transport through pores

(iii) Li^+ intercalation

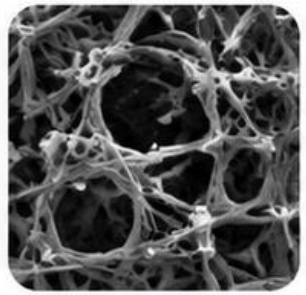

Porous electrode microstructure

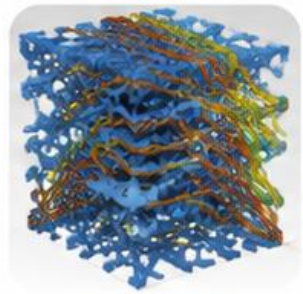

Tortuosity & ion pathways

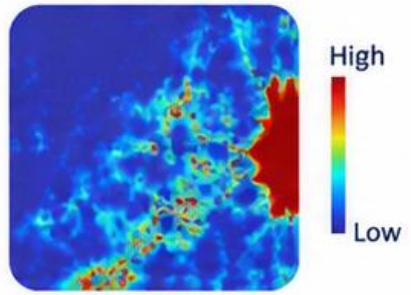

Through-plane ion transport

Key References

- Cooper, S. J. et al. TauFactor: An open-source application for calculating tortuosity factors from tomographic data. SoftwareX 5, 203–210 (2016).
- Tjaden, B., Bergt, D. L. I. & Shaering, P. R. Tortuosity in electrochemical devices: a review of calculation approaches. Int. Mater. Rev. 63, 47–67 (2018).
- Ebner, M. et al. K-rigA Tomography of Porous, Transition Metal Oxide Based Lithium Ion Battery Electrodes. Adv. Energy Mater. 3, 845–850 (2013).

Laser-engineered porous architectures

Architectures investigated in literature:

- Cylindrical wells
- Conical wells
- Linear patterns
- Triangular arrays
- Grid structures

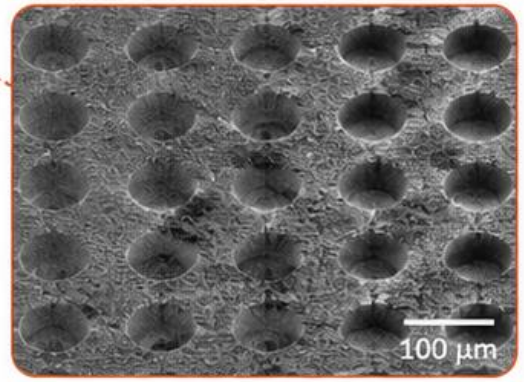

Dasgupta Niels Michigan–paper image

Architecture implemented in lab:

- Upper electrode region selectively modified
- Bottom region preserved intact
- Enhanced transport while maintaining mechanical and electrical integrity

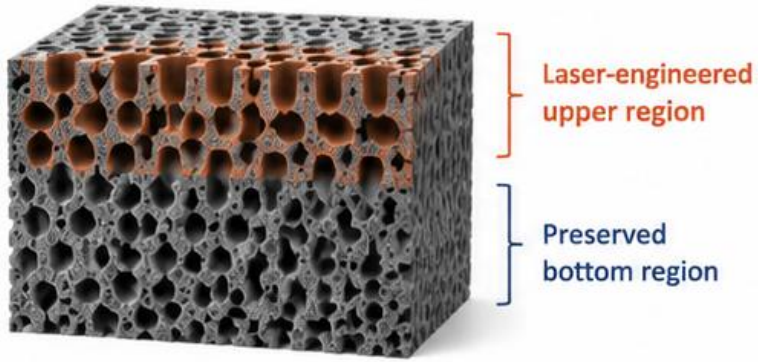

Lased electrode:

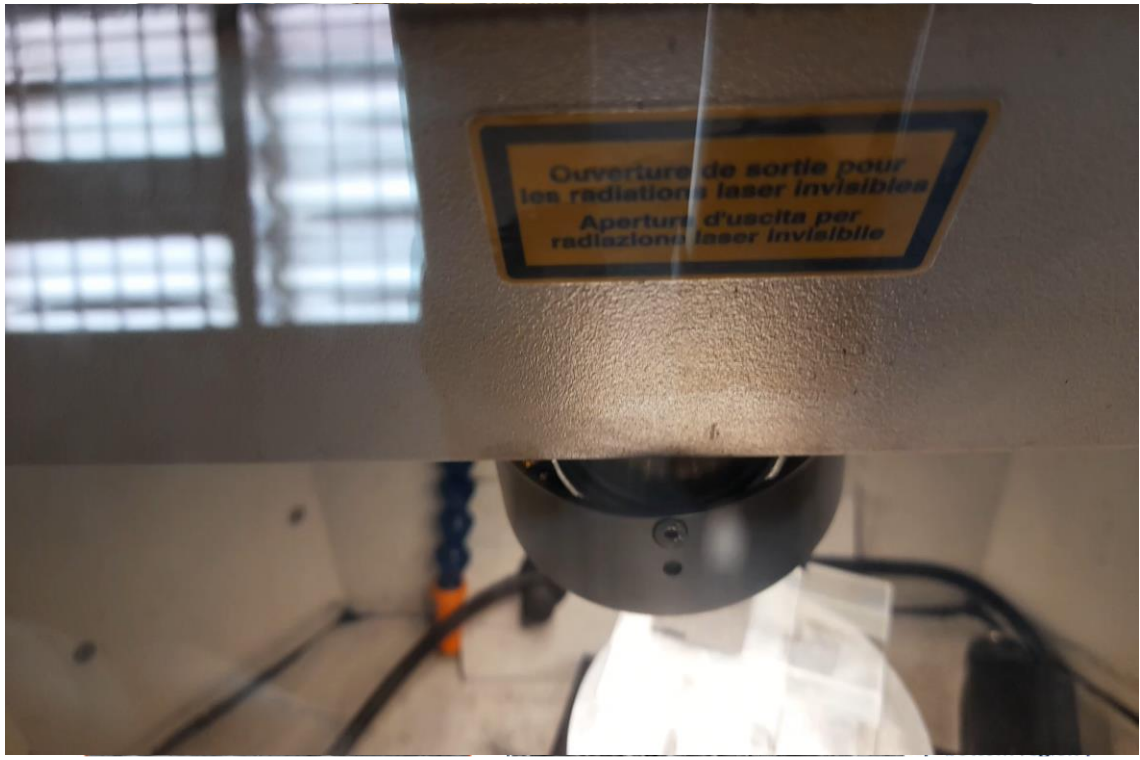

Key References

Phlypo, W. A. review of laser electrode processing for development and manufacturing of lithium-ion batteries. *Nanophotonics*, 7, 569–575 (2018).
Habeebank, J. B. et al. Enhanced Fast Charging and Reduced Lithium-Plating by Laser-Structured Anodes for Lithium-Ion Batteries. J. Electrochem. Soc. 166, A3904–A3949 (2019).
Chen, K.-H. et al. Efficient fast charging of lithium-ion batteries enabled by laser-patterned three dimensional graphite anode architecture. *J. Power Sources* **471**, 228475 (2020).

Partial laser scanning strategy leads to enhanced capacitance

At highest scan rate (0.20 V s^{-1})

- Tr-210 80.3%
- Tr-205 31.4%
- Tr-200 19.5%
- Untreated 14.7%

Capacitance retention relative to 0.01 V s^{-1}

Gravimetric electrode capacitance

(1 M Na_2SO_4 aqueous electrolyte)

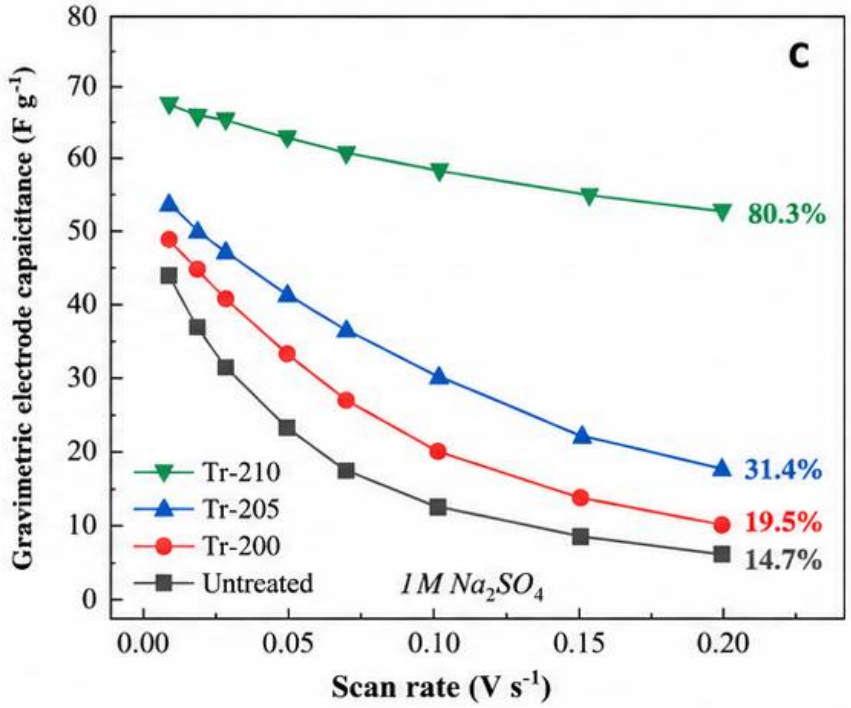

Cyclic voltammetry (scan rate = 30 mV s^{-1})

(1 M Na_2SO_4 aqueous electrolyte)

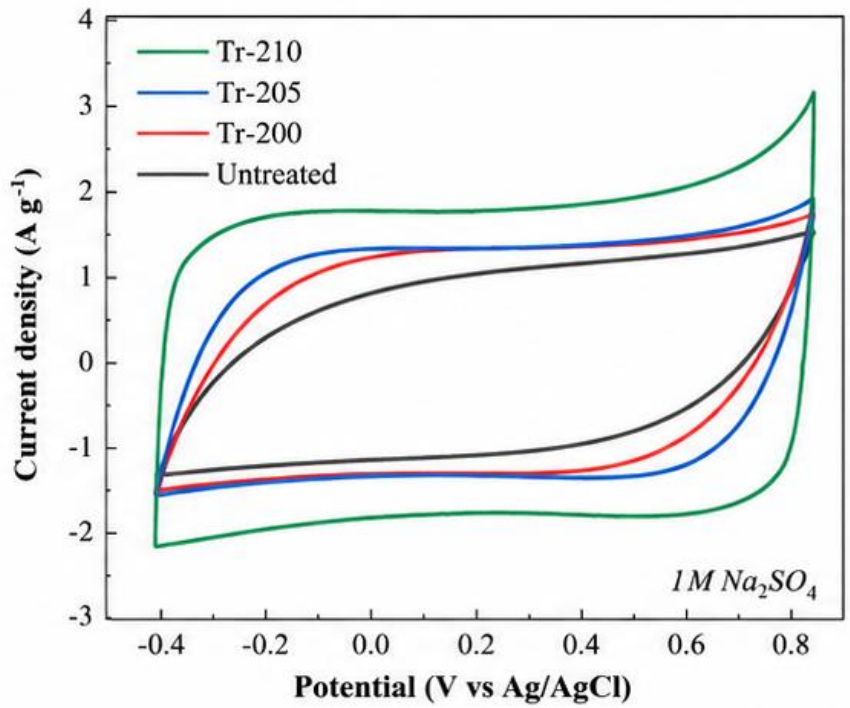

Key takeaway

- Higher capacitance at all potentials
- Larger enclosed area → Higher charge storage
- Improved ion transport kinetics

Laser-modified upper region

Preserved bottom region

PUBLICATION UNDER REVIEW

Partial laser scanning generates a high-surface-area upper region that reduces ion transport path lengths, leading to significantly enhanced capacitance, especially at high scan rates.

Athinais

Partial laser scanning strategy enhances fast charging

Partial laser restructuring creates a **high-surface-area upper region**, improving ion accessibility and enabling superior high-rate performance.

a Graphene anode

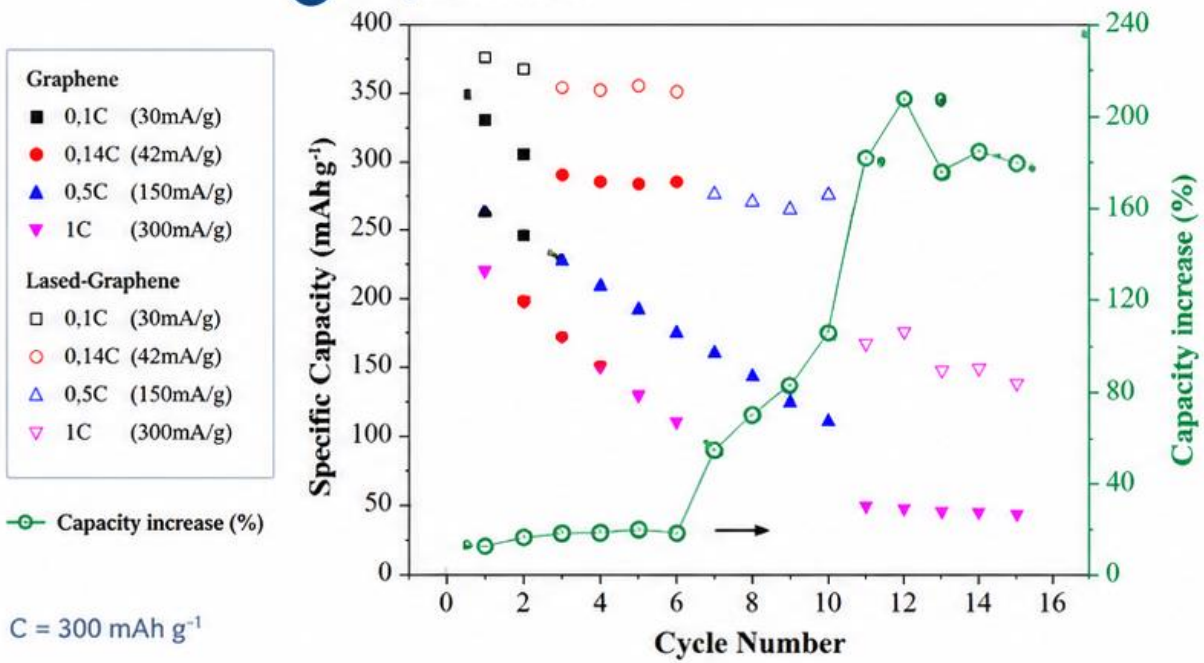

C = 300 mAh g^{-1}

b Graphite anode

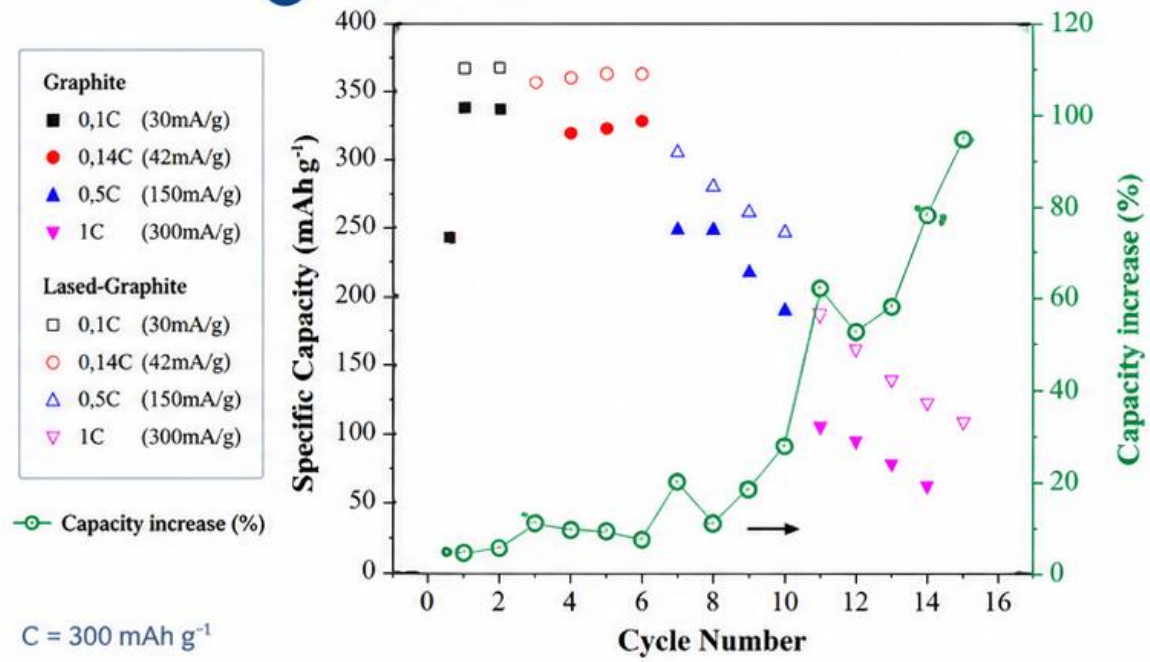

C = 300 mAh g^{-1}

Higher accessible capacity across all rates (0.1C–1C)

Up to **~200% increase** in capacity at high C-rates (graphene anode)

Significant improvement in **fast-charging performance** for both graphene and graphite

Key takeawy

Partial laser scanning effectively restructures the anode surface, unlocking **accessible porosity** and enabling **superior rate capability** for fast charging.

Publication under review

A scalable laser-assisted method for restructuring the surface of graphite/graphene anodes in Li-ion batteries to enhance accessible porosity and high-rate performance.

M. Athanasiou[1†], D. Roumelioti[2†], D. Hoxha[1], K. Mylonas[3], V. Dracopoulos[3], E. Bellou[1], L. Sygellou[1], N. Bali[1] and S. N. Yannopoulos[1,2†]

Computational workflow

Enable / Disable

1 **Structure image**
Tomographic or FIB-SEM data

2 **3D reconstruction**
Segmentation and volume rendering

3 **Descriptor extraction**
Quantify geometry and topology

4 **Transport simulation**
Solve transport through pores

5 **Performance evaluation**
Predict electrochemical performance

DESCRIPTORS EXTRACTED

Tortuosity
Path complexity of pores

Connectivity
Pore network interconnection

Anisotropy
Directional variation in structure

Dead-end fraction
Fraction of isolated pore ends

This integrated workflow links 3D microstructure to electrochemical performance, enabling data-driven design and optimisation of porous battery electrodes.

CARBON BASED ELECTRODE

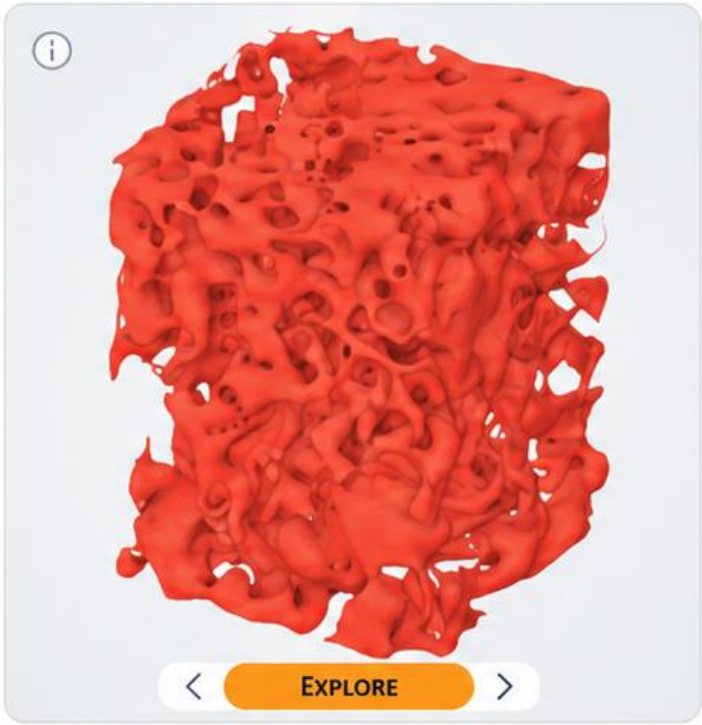

Using Ansys Discovery and Fluent we can estimate the transport properties

Key Microstructural Descriptors — Batch Summary

Distributions across 48 images

Dataset: 48 microstructures (batch_descriptors.csv)

Porosity ϕ

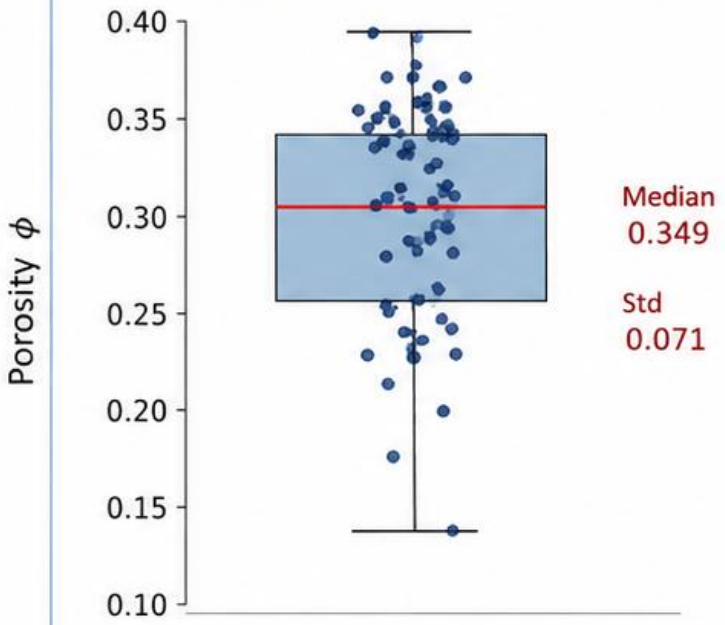

Range: 0.15 – 0.38
Most samples: 0.22 – 0.38

Connectivity (largest cluster)

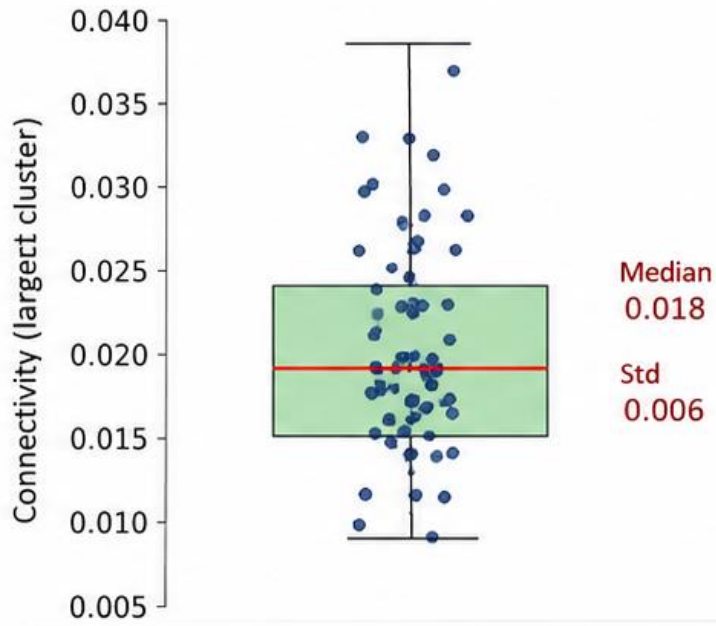

Range: 0.009 – 0.036
Most samples: 0.015 – 0.023

Dead-end fraction ϕ_d

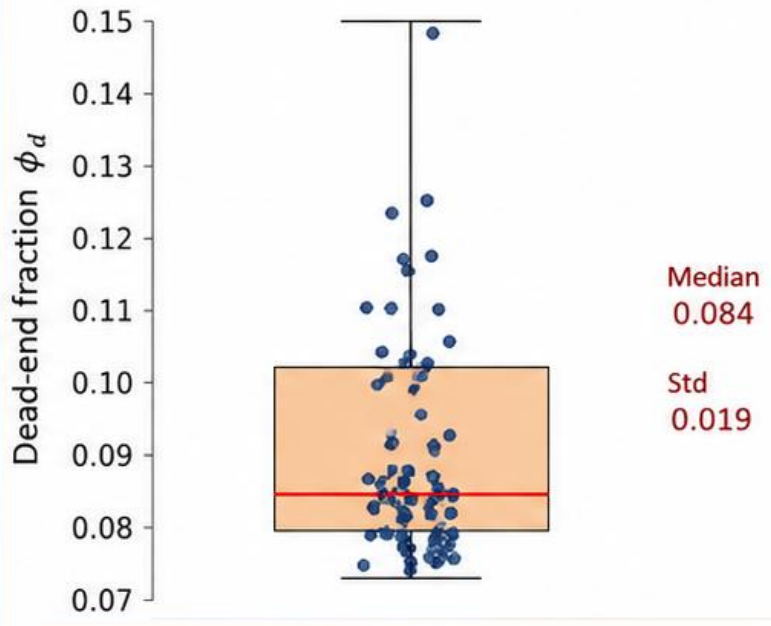

Range: 0.075 – 0.145
Most samples: 0.078 – 0.112

Porosity

Wide variation across the dataset indicating diverse void space availability.

Connectivity

Moderate values with a right tail, reflecting differences in pathway continuity.

Dead-end fraction

Most structures have low-to-moderate dead-end content with a few high outliers.

3D microstructure reconstruction and transport analysis

From 48 images to quantitative transport properties

WORKFLOW

1. **Image acquisition**
   48 cropped SEM images
2. **3D reconstruction**
   Tomographic reconstruction
3. **Descriptor extraction**
   Quantify geometry and topology
4. **Transport simulation**
   Dijkstra's shortest path analysis
5. **Performance evaluation**
   Link microstructure to transport

48 images processed to generate a representative 3D volume and extract transport-relevant descriptors.

1. Cropped SEM (databar removed)

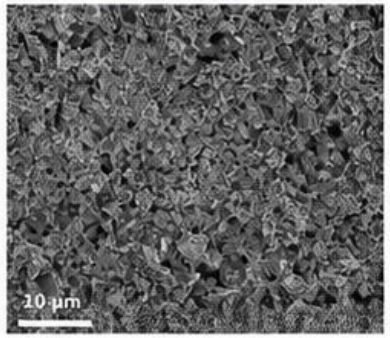

4. Watershed segmentation
2111 individual pores

7. Pore Size Distribution
(+ log-normal fit)

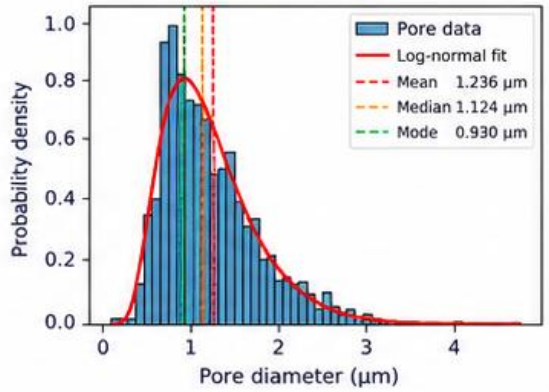

Geometric Tortuosity — Dijkstra's Shortest Path
PL2075-210V10.tif φ=0.3458 τ_x=1.5647 τ_y=1.4537

Dijkstra τ_x (left → right)
τ = 1.5647 | path ≈ 1417 steps straight = 1024 px

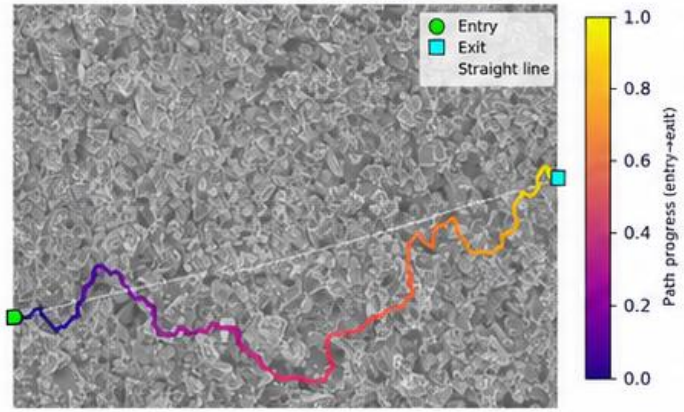

Dijkstra τ_y (top → bottom)
τ = 1.4537 | path ≈ 894 steps straight = 691 px

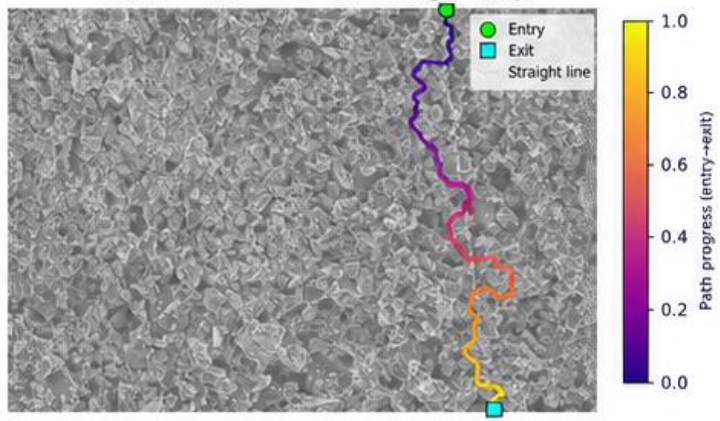

KEY RESULTS

- **Porosity (ϕ)** 34.58 %
- **Tortuosity τ_x** 1.5647 (left → right)
- **Tortuosity τ_y** 1.4537 (top → bottom)
- **Mean pore size** 1.236 µm

KEY TAKEAWAYS

- Watershed segmentation identifies 2111 individual pores.
- Log-normal pore size distribution with a mode at ~0.93 µm.
- Anisotropic transport with slightly higher tortuosity in the x-direction.

Image-based 3D reconstruction enables quantification of pore structure and transport, linking microstructural features to ion transport performance in laser-engineered electrodes.

Linear regression model accurately predicts LOO performance

Model trained on 48 images to predict limiting current density (LOO) from microstructural descriptors

LINEAR REGRESSION MODEL

Predicts LOO limiting current density from microstructural descriptors.

R^2 = 0.9694
Excellent goodness of fit

MAE = 0.0656 J/cm²
Low average prediction error

Strong linear correlation between predicted and actual LOO fluence

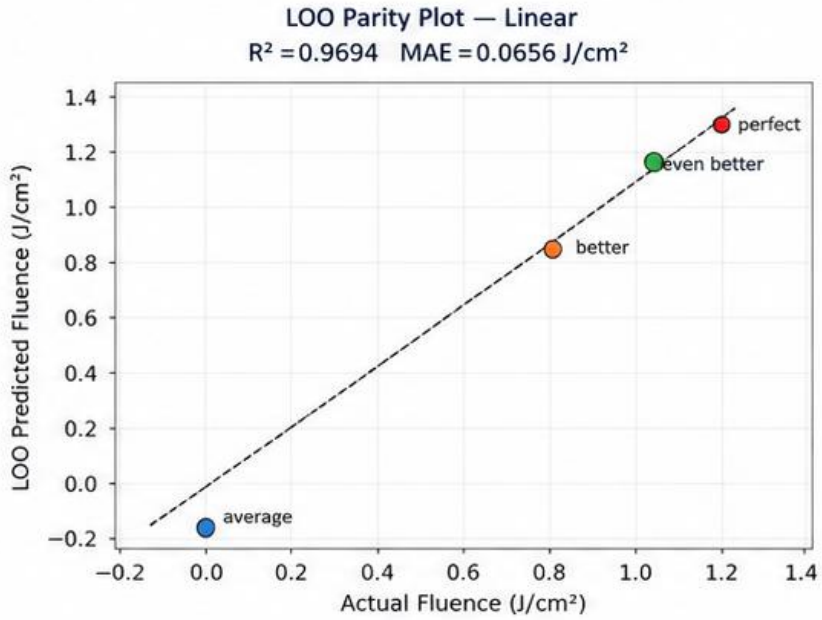

Condition means
- average
- better
- even better
- perfect

Dashed line: perfect prediction

KEY TAKEAWAY

The linear model reliably captures the relationship between microstructure and LOO, enabling fast and accurate performance prediction.

Model advantages

- High predictive accuracy
- Interpretable and computationally efficient
- Generalizes across a wide range of microstructural conditions

All Descriptors vs Fluence
(small dots = images = condition means ± std)

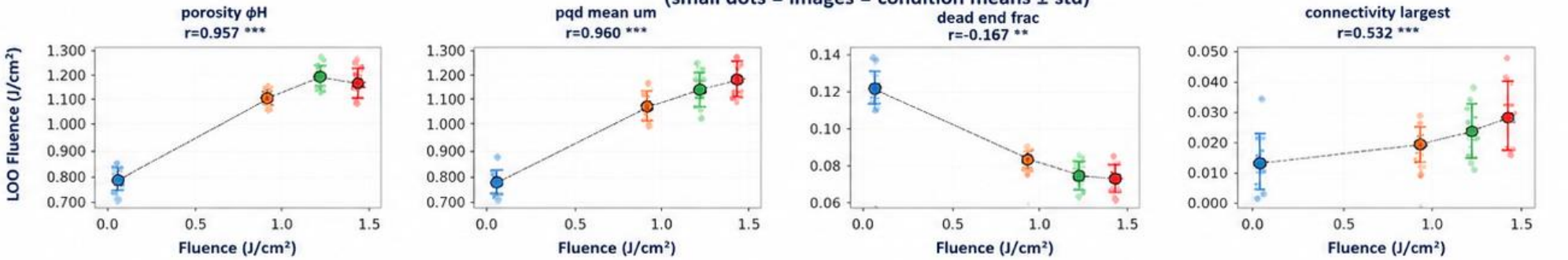

The model demonstrates strong predictive capability across key microstructural descriptors.

Higher porosity and pore size are associated with higher LOO, while dead-end fraction shows an inverse relationship. Connectivity exhibits a positive trend, though with greater variability.

Implication

This data-driven model can accelerate the design and optimization of laser-processed electrodes.

Laser-Assisted Fabrication and Multiscale Optimization of Binder-Free Graphene–Si Composite Anodes for Li-Ion Batteries

Structure-resolved simulations reveal:

1. Phase & Structural Validation (Raman Spectroscopy)

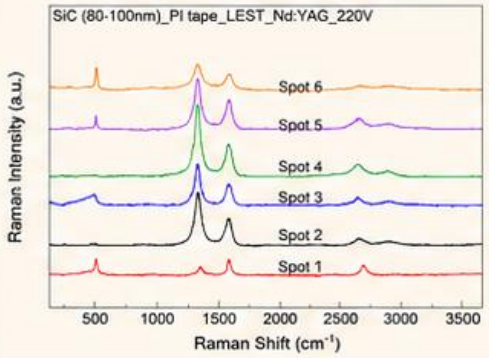

Sample A : Low LASER Fluence / 220V

- ✓ **Presence** of sharp crystalline Silicon peaks at **520 cm^{-1}**.
- ✓ Identification of Graphene **D, G, and 2D** characteristic bands.
- ✓ Coexistence of crystalline Si and Graphene phases.

2. Quantitative Morphological Mapping (SEM)

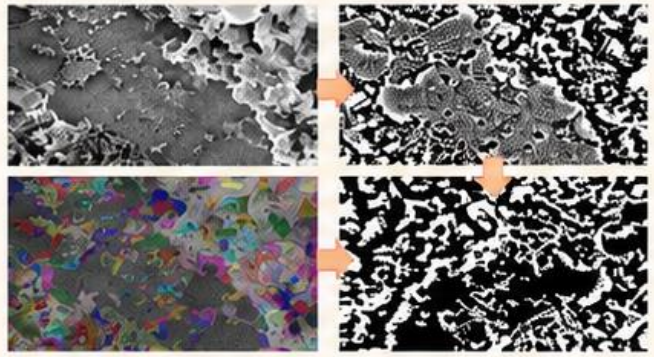

Pores = 147, Porosity = 30.50%

1. Phase & Structural Validation (Raman Spectroscopy)

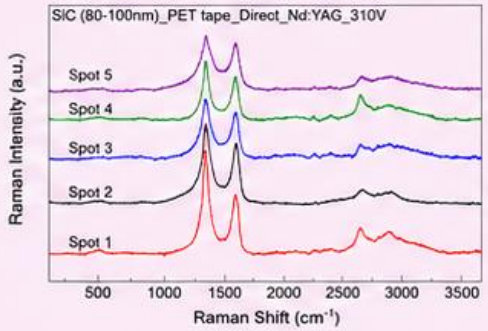

Sample B : High LASER Fluence / 310V

- ✓ **Absence** of crystalline Silicon peaks at **520 cm^{-1}**.
- ✓ Dominant Graphene **D, G, and 2D** signatures across all spots.
- ✓ High-intensity D and G bands suggesting extensive carbon restructuring.

2. Quantitative Morphological Mapping (SEM)

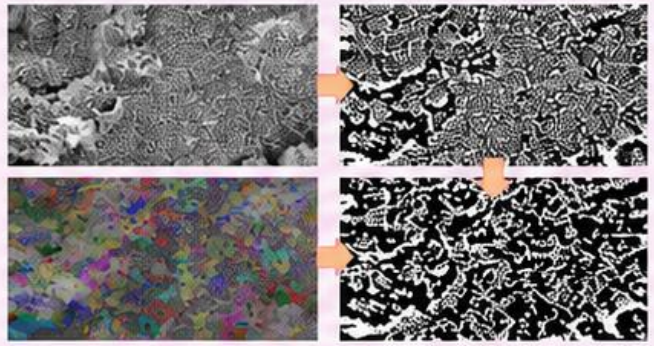

Pores = 177, Porosity = 33.39%

Interesting outcome

Sample chemical analysis led to very controversial results and they were misleading us—we couldn't be sure about precursor material or other laser initial setting/option.

However, when we looked into structure, the electrochemical behaviour started matching with a trend!

This highlights the importance of structure-resolved analysis and multiscale modeling to uncover the true impact of laser processing on electrode performance.

Higher laser fluence drives carbon restructuring, increases porosity, and enhances graphene network connectivity—key factors that ultimately translate into improved electrochemical performance.

Structure tells the truth—and performance follows.

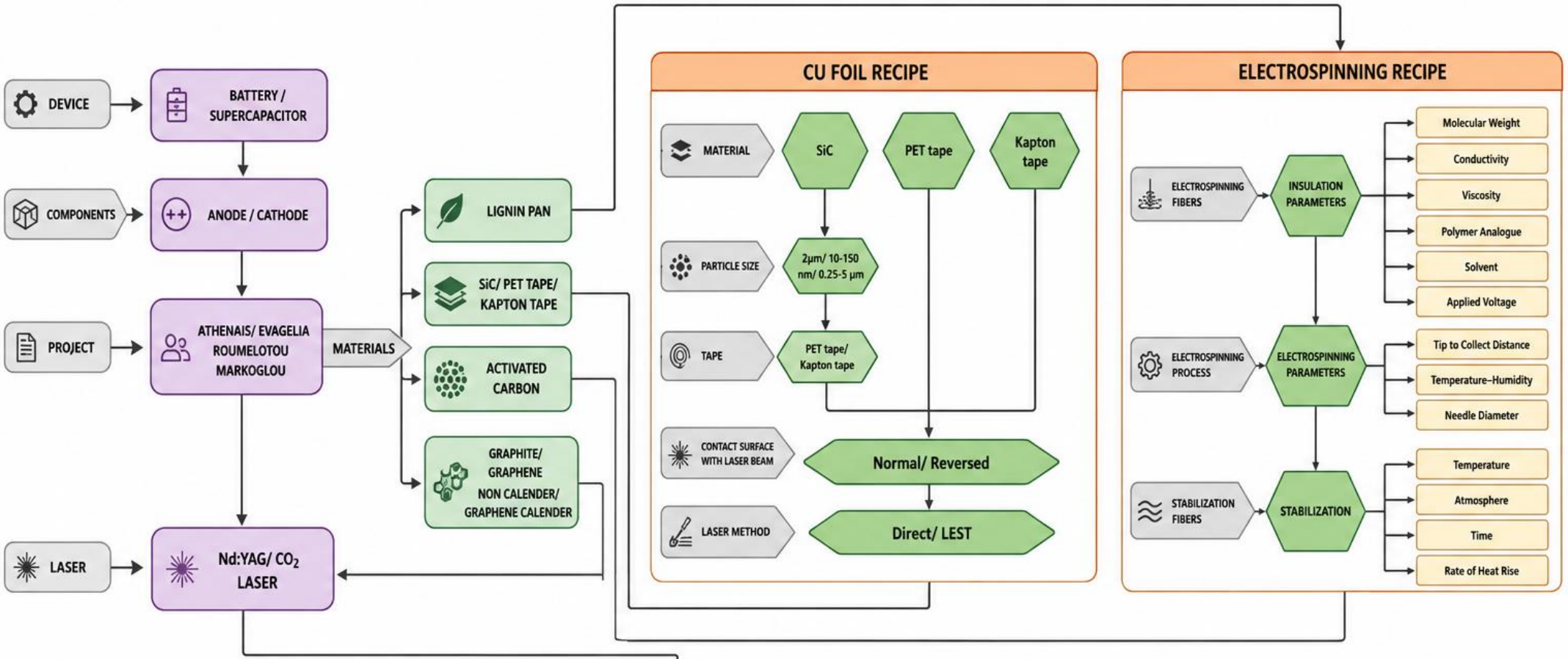

TREATED PARAMETERS

Nd:YAG		CO2	
VOLTAGES (V)	190–320	SCAN SPEED (mm/s)	5–500
PULSE DURATION (ms)	1.5	POWER (%)	0–100
SPOT SIZE (mm)	1.4	INTERVAL (mm)	0.1
HERTZ (Hz)	2	HEAD DISTANCE (mm)	10
STAGR SPEED (mm/min)	910		

Conclusions and Outlook

1 **Pore architecture strongly controls fast-charging behaviour**

Transport pathways, bottlenecks and phase distribution dictate electrochemical performance.

2 **Transport cannot be described by porosity alone**

Connectivity, tortuosity, pore-size distribution, anisotropy and dead-end fraction jointly govern transport.

3 **Structure-resolved descriptors outperform classical effective-medium assumptions**

Realistic porous electrodes exhibit heterogeneous and multiscale transport pathways.

4 **Image-based modelling enables hierarchical optimisation of electrode architectures**

Linking microstructure directly to electrochemical performance for large design spaces.

CONCEPTUAL EVOLUTION OF THIS WORK

1. Physics problem
Fast charging is transport limited

High-rate performance is governed by ion and electron transport in complex porous electrodes.

2. Microstructure analysis
Porosity alone is insufficient

Real microstructures are heterogeneous and multiscale, leading to large transport variability.

3. Descriptor extraction
Tortuosity • PSD • Connectivity
Anisotropy • Dead ends

Quantitative descriptors capture key physical mechanisms and design-relevant information.

4. Predictive modelling
Linear regression validates structure–performance relationships

Strong correlations and high predictive accuracy confirm the importance of architecture.

5. Next step: CNNs
Learn spatial transport signatures directly from microstructure

CNNs capture local morphology, spatial correlations and multiscale patterns beyond handcrafted descriptors.

The transition from handcrafted descriptors to image-based deep learning opens a pathway toward physics-informed autonomous electrode design.

Better structure understanding today drives better batteries tomorrow.

O U T L O O K

Where this work goes next

- Multi-scale architectures (nano- to micro-)
- Extension to Si composite batteries

Acknowledgements

- Athanasios Souliotis
- Athinais Mavrikaki
- Dimitra Roumelioti
- Natalia Kantouni
- Evangelia Tsakali

This work is supported by the European Union, under Horizon Europe Programme GRAPHERGIA (Grant Agreement n.101120832).

Funded by the European Union

Thank you

Questions welcome.

Contacts:
Prof. Spyros N. Yannopoulos (Advance material development) sny@iceht.forth.gr
Michael Athanasiou (Electrochemical methods) m.athanasiou@iceht.forth.gr
Nadia Bali (Models and Simulations) nbali@iceht.forth.gr

Second-order Bruggeman comparison for anisotropic inclusions

Needles vs disks using known D_1, D_2 and phase fractions ϕ_1, ϕ_2

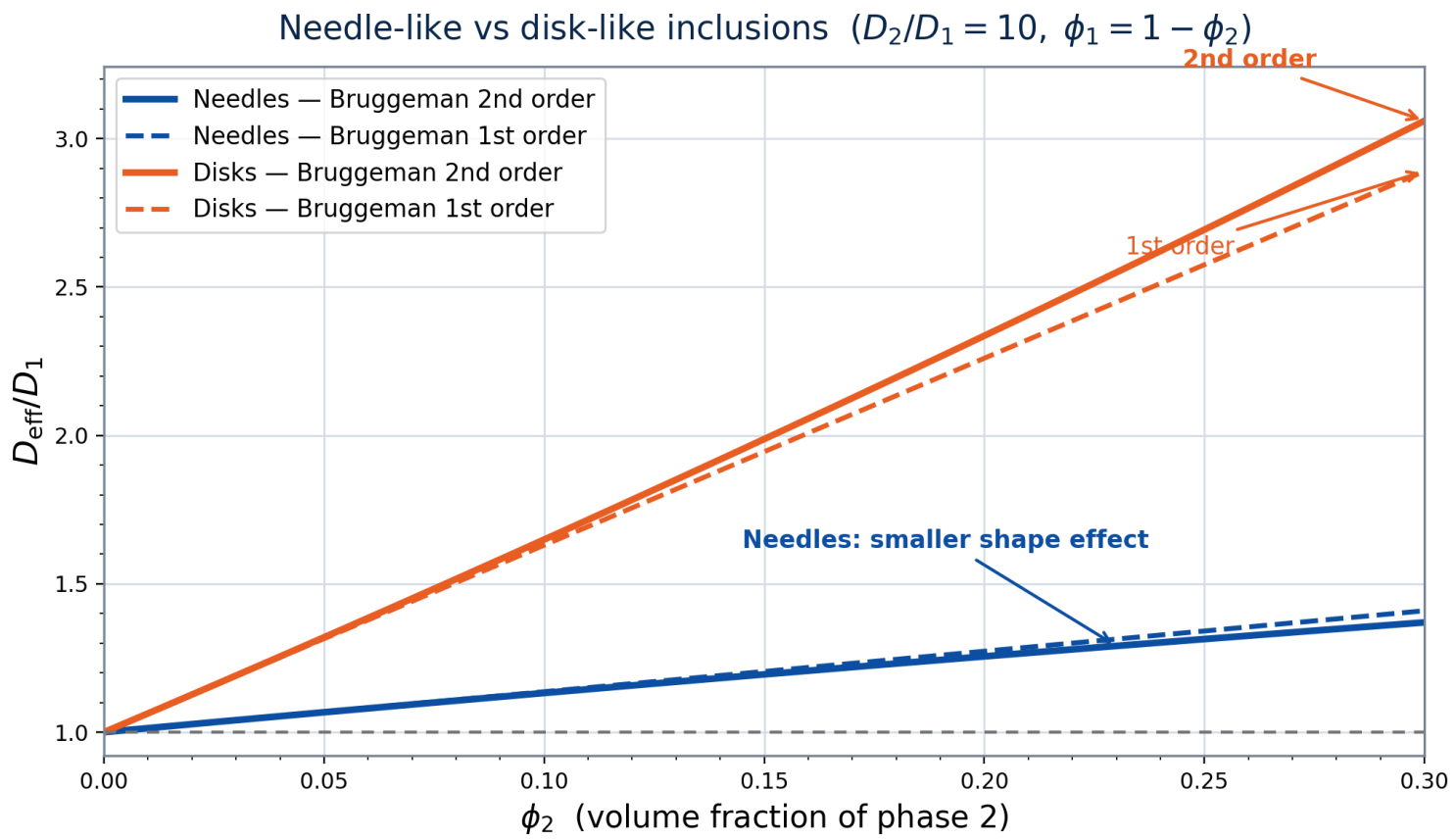

BRUGGEMAN EXPANSIONS

First order $D_{eff} / D_1 = 1 + A \cdot \phi_2$

Second order $D_{eff} / D_1 = 1 + A \cdot \phi_2 + B \cdot \phi_2^2$

Needles $A_n = ((D_2 - 5D_1)(D_2 - D_1)) / (3D_1(D_2 + D_1))$

Disks $A_D = ((2D_2 + D_1)(D_2 - D_1)) / (3D_1D_2)$

$\phi_1 + \phi_2 = 1$; $D_2 > D_1$

B terms are the quadratic coefficients from expanding the same Bruggeman increment to $O(\phi_2^2)$.

OBSERVATION

- Disks show a stronger enhancement when $D_2 > D_1$.
- Second order is close to first order at low ϕ_2, but diverges as ϕ_2 grows.
- Needle-like inclusions remain comparatively less sensitive to ϕ_2 for this contrast.

✓ **Add the second-order term to visualize when dilute Bruggeman predictions begin to depart from the linear approximation.**

Use the same plot with your measured D_1, D_2 and ϕ_2 range to compare against the microstructure-based transport simulations.

Laser restructuring increases accessible porosity

Partial laser scanning
significantly enhances the accessible porosity of both graphene and graphite electrodes.

KEY OBSERVATIONS

Large increase in high porosity
Lased graphene and lased graphite show substantially higher porosity.

Wider porosity distribution
Laser processing introduces a broader pore size population and hierarchical structure.

More beneficial for graphene
Greater relative improvement compared to graphite.

Porosity measured from 3D reconstructions using image-based analysis.

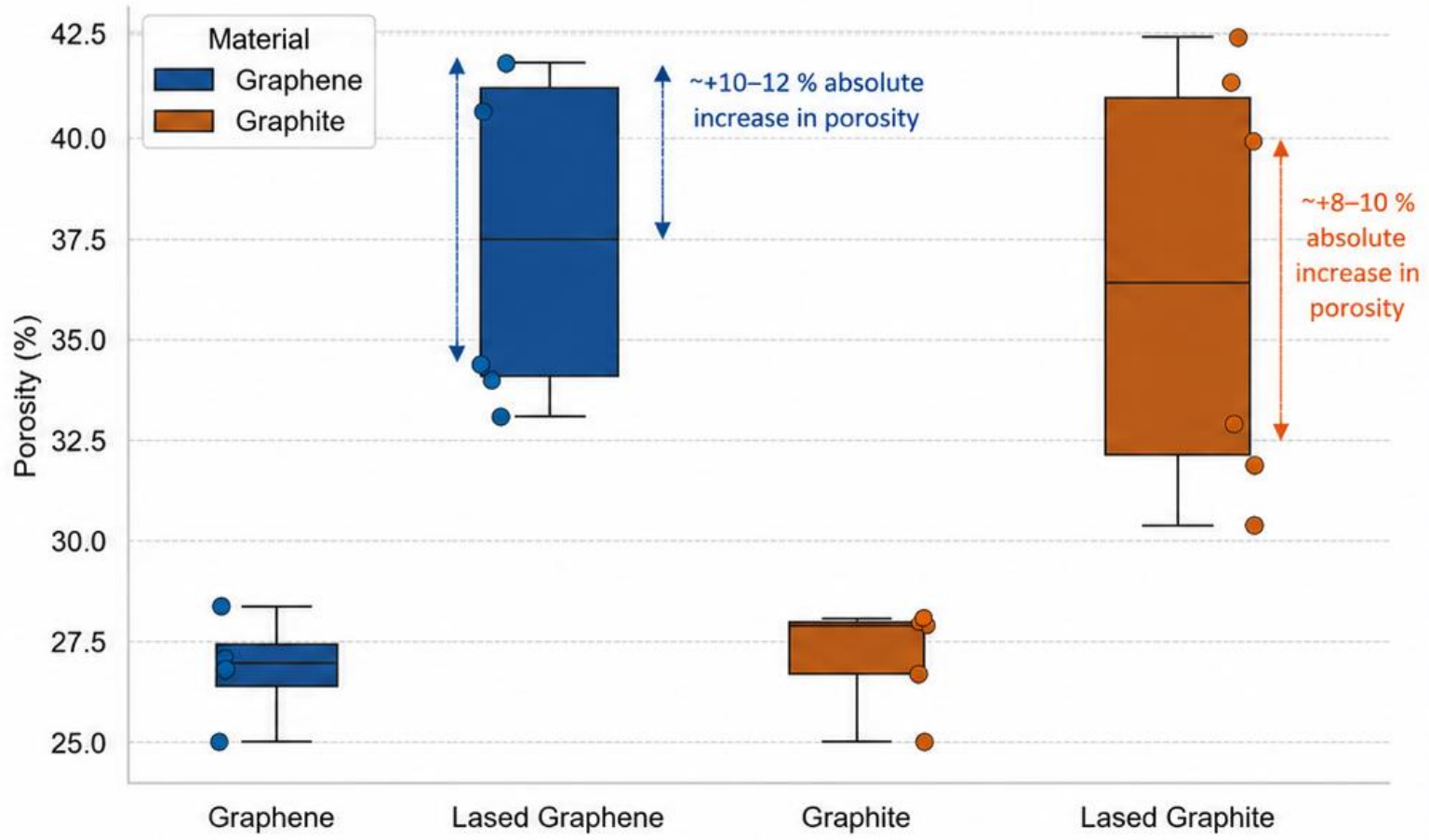

Laser restructuring effectively unlocks accessible porosity,
providing more open pathways for ion transport and enabling enhanced high-rate performance.